PROCEEDINGS OF SCIENCE

Observational Challenges on the ISS: A Case Study with CALET

Nicholas Cannady[a,b,c,*] **and Yuta Kawakubo**[d] **for the CALET collaboration**

[a] *Center for Space Sciences and Technology, University of Maryland, Baltimore County, 1000 Hilltop Circle, Baltimore, Maryland 21250, USA*
[b] *Astroparticle Physics Laboratory, NASA/GSFC, Greenbelt, Maryland 20771, USA*
[c] *Center for Research and Exploration in Space Sciences and Technology, NASA/GSFC, Greenbelt, Maryland 20771, USA*
[d] *Department of Physics and Astronomy, Louisiana State University, 202 Nicholson Hall, Baton Rouge, Louisiana 70803, USA*

E-mail: `nicholas.w.cannady@nasa.gov`

The International Space Station (ISS) provides an orbital platform for astrophysical missions with lower resource requirements than free-flying satellites. The many uses of the ISS, how7 keVever, can produce unique challenges to the accurate analysis of the data acquired by these instruments. In this work, we present effects observed by the Calorimetric Electron Telescope (CALET), an astroparticle physics mission installed on the Japanese Experiment Module Exposed Facility of the ISS. The CALET calorimeter is sensitive to cosmic-ray electrons and gamma rays from 1 GeV up to above 10 TeV, and to cosmic-ray hadrons up to PeV total energies. The CALET Gamma-ray Burst Monitor (CGBM) is sensitive to X-rays and low-energy gamma rays from 7 keV to 20 MeV. Furthermore, ultra-heavy galactic cosmic-ray (UHGCRs) abundances are measured by CALET using a much more open geometry than is possible for events which shower in the instrument. In this work, we discuss ISS-related issues that affect the observations by CALET. Here we detail the ways these effects are accounted for in the production of scientific results. Finally, the possible impact on future missions such as TIGERISS (Trans-Iron Galactic Element Recorder for the International Space Station; planned for deployment to the ISS in 2026) and mitigation strategies are discussed.

38th International Cosmic Ray Conference (ICRC2023)
26 July - 3 August, 2023
Nagoya, Japan

ICRC2023
38th International Cosmic Ray Conference
The Astroparticle Physics Conference

PoS(ICRC2023)063

---

[*] Speaker

https://pos.sissa.it/

1. Introduction

The International Space Station (ISS) provides a unique platform for space-based experiments representing a broad range of scientific inquiry. As a platform with lower cost and lower risk than a free-flying satellite, it is an accessible option with existing infrastructure for a variety of mission classes. A number of astrophysics missions have called the ISS home, including (but not limited to) the Calorimetric Electron Telescope (CALET), the Alpha Magnetic Spectrometer (AMS-02), the Monitor of All-sky X-ray Image (MAXI), and the Neutron star Interior Composition Explorer (NICER). In this work, we focus on lessons learned in the operation of the CALET experiment regarding environmental challenges associated with the ISS. We discuss the observational difficulties posed in each case and the strategies that were adopted to mitigate them. Finally, we briefly present the upcoming Trans-Iron Galactic Element Recorder for the ISS (TIGERISS) mission (accepted in the NASA Astrophysics Pioneers program in 2021; slated for deployment in 2026) and the expected impact of the previously discussed challenges on TIGERISS science.

2. The CALET instrument

CALET [1] is an astroparticle physics experiment with two on-board instruments: the deep electromagnetic calorimeter for measurement of cosmic-ray electron and gamma rays in the GeV–TeV range, and of cosmic-ray protons up to PeV total energies; and the CALET Gamma-ray Burst Monitor (CGBM) for detection of Gamma-Ray Bursts (GRBs) and other transients in the keV–MeV energy range. The CALET payload was launched in August 2015, was installed on the Japanese Experiment Module Exposed Facility (JEM-EF) shortly thereafter, and has maintained stable scientific data collection since October of that year.

The CALET calorimeter comprises three detector subsystems: the Charge Detector (CHD), the Imaging Calorimeter (IMC), and the Total Absorption Calorimeter (TASC). The CHD is two layers of 14 plastic scintillating paddles, arranged in crossed orientation such one samples the X-direction spatially and the other samples the Y-direction. The IMC is eight pairs of crossed layers of 448 fine plastic scintillating fibers (< 1 mm^2) each, with 7 sheets of tungsten providing a passive target between the eight pairs. This gives a normal incidence depth of 3 radiation lengths in the IMC such that electron or photon primaries largely interact early enough in the IMC to provide a clear picture of the shower development for track reconstruction and shower analysis. Finally, the TASC is 12 alternating X-Y layers of 16 lead tungstate (PWO) logs each, with a total normal incidence depth of 27 radiation lengths. Electromagnetic showers up to several TeV can be fully contained in the TASC, giving a fine energy resolution up to these energies. Whereas the calorimeter provides a total of 30 radiation lengths for electromagnetic showers, it is only 1.3 proton interaction lengths deep, usually leading to a single hadronic interaction for nuclear primaries. Showers from cosmic-ray nuclei therefore have a different shower topology than those from electromagnetic primaries, and measured quantities based on the shower development and shape can be used to distinguish between these event classes.

The calorimeter supports up to three simultaneously active hardware triggers at any one time [2]. For primary science, the high-energy (HE) trigger mode is generally always active (~86% live time fraction, largely driven by ~5 ms dead time per triggered event) with an effective energy

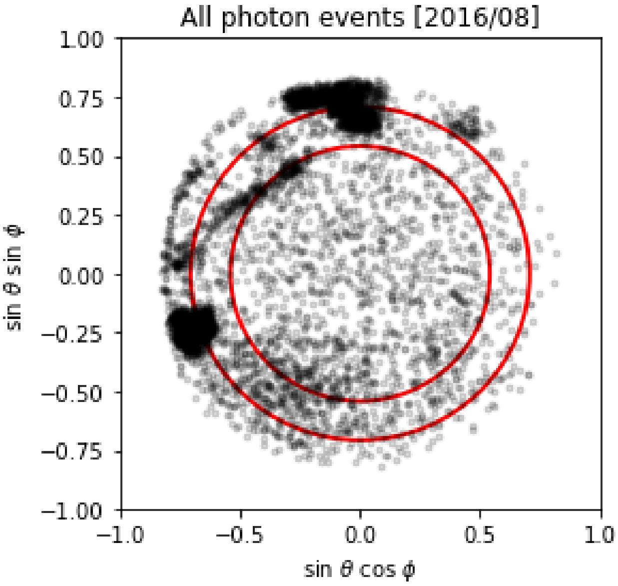

Figure 1: All photon events in the CALET FOV for the month 2016/08. Individual gray dots are photon events, and the inner and outer red circles indicate 45° and 60°, respectively.

threshold for electrons of ~10 GeV. A dedicated ultra-heavy (UH) trigger mode is also used with a high duty cycle, with high thresholds in the IMC only to allow for detection of non-interacting nuclei heavier than boron over a very large acceptance. A variety of other secondary science and calibration modes are also used, including a low-energy gamma-ray (LEG) trigger mode for detection of photon primaries down to ~1 GeV at low geomagnetic latitudes, a low-energy electron (LEE) trigger mode for detection of electron primaries down to ~1 GeV at high geomagnetic latitudes, and calibration modes for regular monitoring of the instrument performance.

CGBM [3] uses inorganic scintillators for the detection of lower-energy photons: a Hard X-ray Monitor (HXM) with two cylindrical pieces of Ce-doped lanthanum bromide ($LaBr_3$) and a Soft Gamma-ray Monitor (SGM) comprising a single cylindrical piece of bismuth germanate (BGO). HXM and SGM both feature photomultiplier tube readouts and are sensitive to photons in the energy ranges 7–1000 keV and 100 keV–20 MeV, respectively. While the calorimeter is able to take data continuously throughout the orbit, CGBM is inactive at high geomagnetic latitudes and in the South Atlantic Anomaly (SAA) where the low-energy particle background would overwhelm and damage the instrument. When both instruments are active, the detection of a transient in CGBM provokes the LEG mode to temporarily become active in the calorimeter (if it is not already active) such that potential emission in GeV-energy gamma rays can be probed [4].

3. Field-of-view obstructions

The first and most impactful effect from the ISS on CALET observations is the presence of other objects in the field of view (FOV). Three types of structures are seen by CALET: fixed, regularly appearing, and irregularly appearing objects. The first class, fixed objects, are easily seen and characterized. For instance, the attachment point to the JEM-EF is seen in the extended

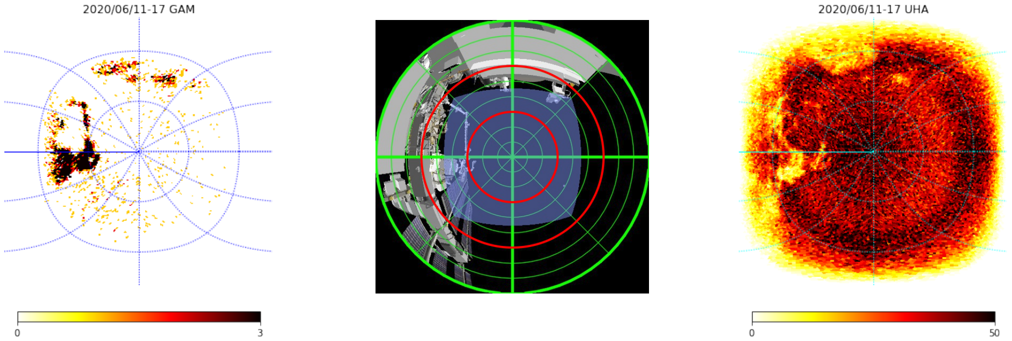

Figure 2: One week in 2020/06 with a large obstruction (SSRMS) visible in the left side of the FOV. From left, the frames show the excess in photon events, a JAXA-provided render of the expected position of the arm during this time period, and the shadow in UH events. Note that the projection is slightly different in the middle frame as opposed to the outer two. The two circles in the graticules for the left and right frames and the red circles in the middle frame mark 30° and 60°, respectively.

FOV available to the LEG (~60°) and UH (~80°) triggers. The second class, regularly appearing objects, are generally associated with standard station operations. These include the solar panel arrays, radiators, and other parts of the station which move within a known range. The final class, irregularly appearing objects, are the most significant. These include the robotic arms (i.e. SSRMS and JEM-RMS), objects being staged or moved in installation or other activities, and CubeSat releases.

Regardless of which of the three classes detailed above a given object comes from, the effects are the same to a greater or lesser extent. Low-energy photons, such as those detected by CGBM, can be largely absorbed by material between the source and the detector, meaning that the sky is shadowed by obstructions (thin enough objects, such as the solar panel arrays, can be thin enough to still allow detection of bright bursts). Cosmic rays can interact in the obstructions, removing some from the observed flux and creating a very bright background of secondary photons which can reach GeV energies. It is through this secondary photon background that the structures can be most clearly seen. An example is given in Figure 1, where individual photons are indicated by transparent gray circles. The center of the FOV is largely unobstructed, while several effects are seen beyond the 45° line. Indicating regions as if the FOV were a clock face, there are strong obstructions at 12:00 and 8:30 which are due to persistent, fixed structures. In the quadrant from 9:00 to 12:00 there is a linear enhancement due to a robotic arm parked in the FOV for ~5 days out of this month. Finally, a diffuse enhancement is seen from ~5:00 to ~8:00 due to frequent rotation of the solar arrays through this region.

In addition to the excess seen in low-energy gamma rays, exploration of the data collected with the UH trigger also revealed the shadow of these highly-charged events clearly. Figure 2 shows both signatures along with a render of the expected activity during a multi-day operation in June 2020. Note that the UH trigger (right frame), with a much wider FOV than even the LEG trigger (left frame), is able to show a large amount of structure. The JEM-EF is at the top of the frame, while the structure on the left side shows the truss, the solar arrays, and the radiators. The SSRMS is parked in the top left quadrant of the FOV, appearing as a two-segment linear obstruction with a

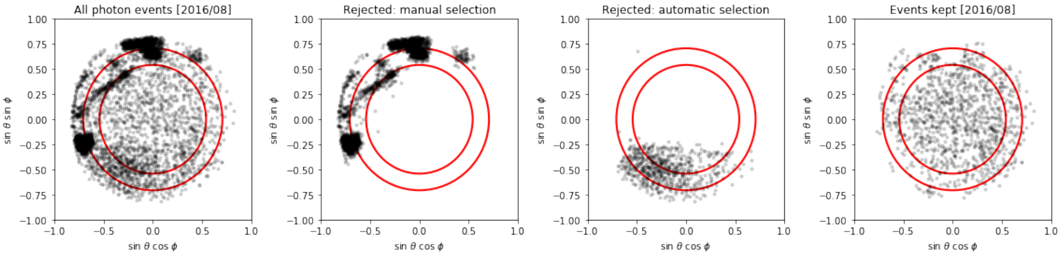

Figure 3: Removal of obstructions. In the leftmost image, all LEG photons are shown. The second and third images show the events removed by the manually-defined daily/monthly filters and the automatic screening, respectively. In the final image, the remaining events are shown. Red circles indicate 45° and 60°, respectively.

larger feature at one end. Note that the ring feature in the full FOV at ~60° in the UH frame is not due to any obstruction, but is an artifact of lower charge nuclei (specifically CNO) at large zenith angles depositing enough energy in the IMC layers to satisfy the UH trigger.

These obstructions are mitigated in two complementary ways. The solar arrays and radiators, which are relatively quickly moving in the FOV, are modeled using ray-tracing software from JAXA. These events are flagged in the generation of the Level 2 data in an automated screening. The events from fixed and irregularly appearing objects are identified manually by visual inspection of monthly and daily maps using the LEG trigger data with a simple photon selection. Monthly maps are templated to remove the persistent structures with small tweaks for objects that move slightly. Daily maps are used to identify conservatively regions where objects are parked or working on each given day, although for many days the monthly map is sufficient. Hourly count rates are also monitored as a secondary check on these cuts, as the rates from the secondary photons are considerably higher than those of astrophysical gamma rays. When high rate hours are identified even after application of the FOV cuts, the daily maps are further scrutinized to remove the offending region.

Flagged regions are logged in the calibration database and used in the selection of events and the calculation of exposure and effective acceptance. This ensures that the regions are fully disregarded in scientific analysis. This has been applied to the analysis of both gamma rays and cosmic rays, although the effect on the obtained spectra of cosmic ray nuclei is found to be small.

4. Radiation background

Early observations with CGBM revealed an interesting step-function feature in the background rates (see Figure 4). The timing of these changes was investigated and found to correspond to docking and departure times of the Soyuz vehicles used to transport people and supplies to and from the station and to perform orbit boosting. Due to the use of a strong gamma-ray source as an altimeter in the Soyuz, these represent a local source of background photons. In Figure 4, it can be seen that when a Soyuz vehicle is not present on the Poisk module, a moderate decrease is seen in the count rates. Furthermore, if none is present on the Rassvet module, an even more significant decrease is found due to its closer proximity to the JEM-EF. As long as these changes in background rate are understood and accounted for, this background does not pose a problem for CALET operations.

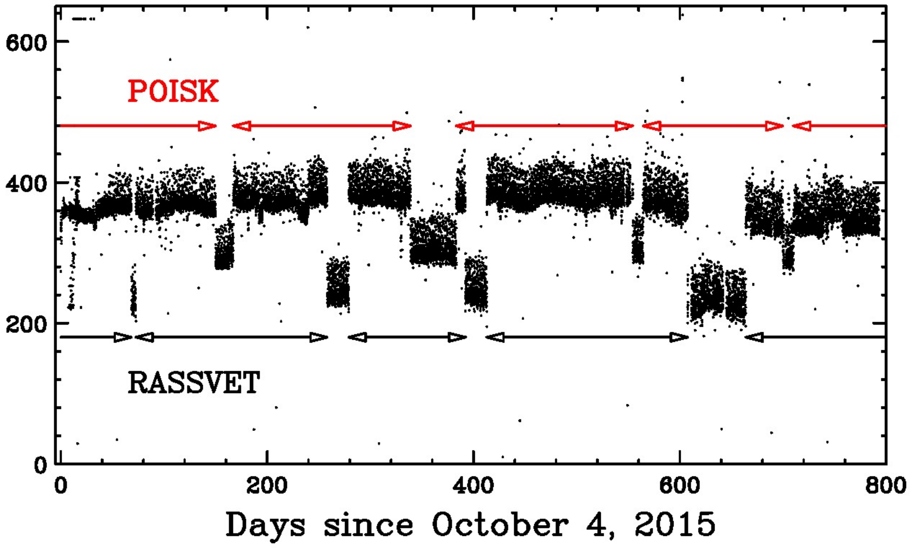

Figure 4: CGBM SGM count rates for 2015/10-2017/12. Red and black horizontal lines indicate times that Soyuz were docked on the Poisk and Rassvet modules.

5. Orientation changes

CALET was designed to be a zenith-pointing instrument to view the sky most optimally. For the majority of time, this is approximately the case (long term deviations are seen at a scale generally smaller than 5° and are well understood). Maneuvers such as docking, however, require the station to change orientation for a short period of time. On very few occasions, more significant deviations are seen that require consideration in data analysis.

Figure 5 shows diagnostic data for three representative days. For each day, a time series plot and three tracking plots are given for the location of the local zenith (i.e. the anti-Earth direction) are presented in the coordinates of the CALET FOV. For the time series plots, a polar angle and an azimuthal angle are shown for the local zenith position by the black and red curves, respectively. These illustrate the magnitude and time over which any significant changes happen. The polar plots show three levels of zoom for the track the local zenith makes across the CALET FOV. The topmost plot is for 2021/07/17 and shows typical behavior. Small fluctuations are seen in the time series plot with a total variation on the order of 1°, and the track on the FOV is very confined. The middle set of plots is for 2019/12/31, and shows the motion as for a standard reorientation for docking, etc. A tilt to ~90° is seen for a time period no longer than an hour. Examining the polar plots reveals a smooth transition from small variations to the tilted position and the return to standard orientation. Finally, the bottommost plot shows an exceptional day, 2021/07/29. A vehicle thruster misfire erratically skewed the orientation of the station for several hours, with CALET pointing nearly directly downwards for a short period of time. A return to the standard orientation was achieved within 12 hours of the initial incident.

In general, the periods of time for which CALET is not (nearly) zenith pointing are quite short, and the effect of the maneuvers on scientific data analysis is minimal. In sensitive analyses these time periods (or even days) can simply be excluded from the data sample with a relatively small

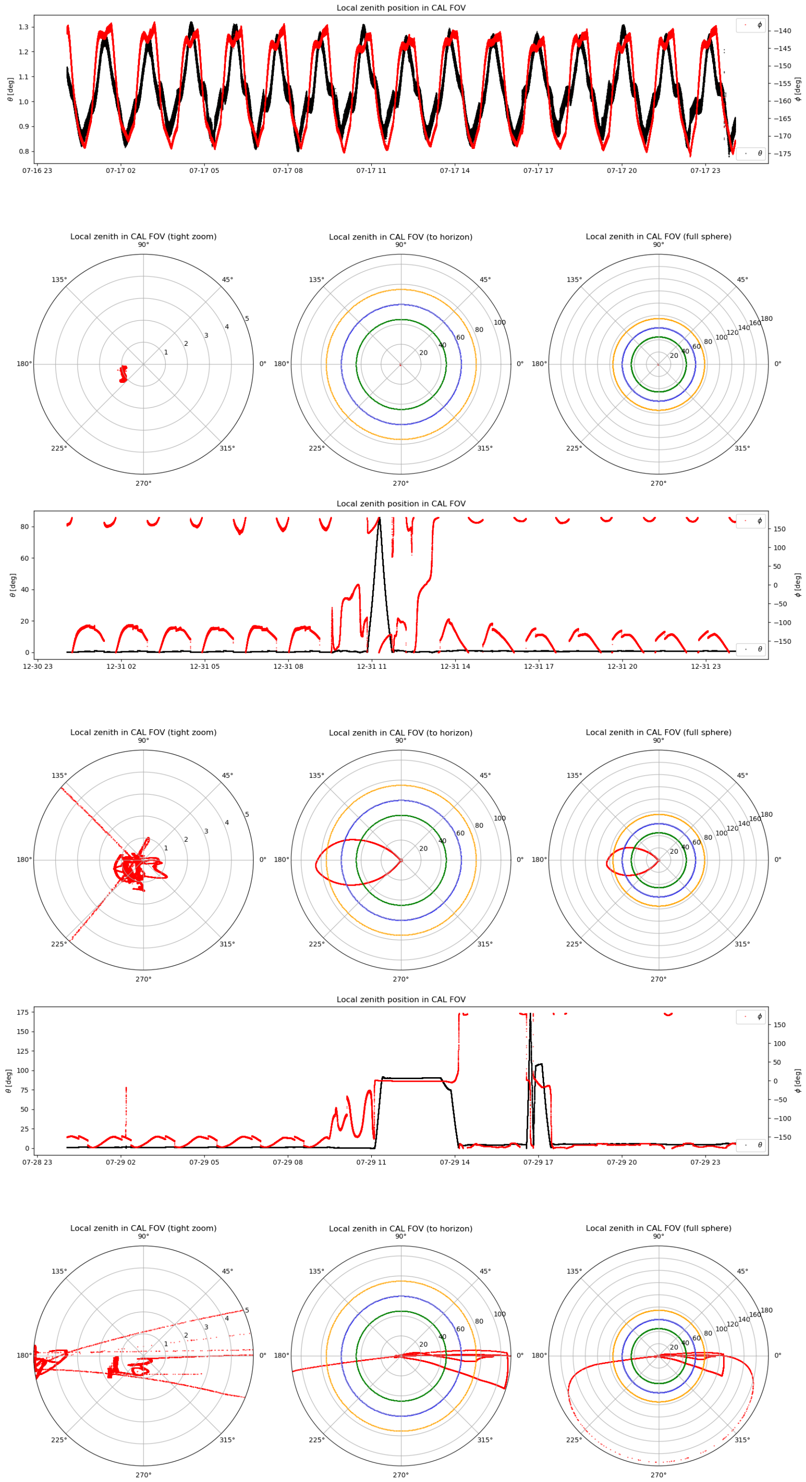

Figure 5: Three days demonstrating range of orientation changes in a short time. For each day, the motion of the local zenith in the CALET FOV is shown. In the horizontal plots, a time series is shown with the black and red curves showing altitude and azimuthal angles, respectively. In the three circular plots, the track of the zenith is shown at three different zoom levels. Top: 2021/07/17, normal behavior; middle: 2019/12/31, rotation of ~90° to accommodate docking; bottom: 2021/07/29, erratic rotation due to docked vehicle misfire.

impact on exposure. These times are also being considered for science topics normally not available to CALET due to zenith pointing (e.g. observations of the Earth limb, etc.).

6. Relevance to TIGERISS

TIGERISS [5] is the latest addition to the TIGER family of instruments, which includes the highly successful balloon-borne TIGER and SuperTIGER experiments. The primary science goal of these missions is the measurement of the relative abundances of heavy (above ~CNO) and ultra-heavy cosmic rays (above Fe). TIGERISS will build on the results of SuperTIGER with improvements to the detector technology by using silicon strip detectors (SSDs) instead of plastic scintillators. These have been tested in a beam exposure at CERN and demonstrated to have very fine charge resolution up to Pb, whereas the charge measurements on previous instruments have saturated or been necessarily grouped into even and odd charges due to worsening resolution. Furthermore, observations above the atmosphere will reduce systematics on the measurement by removing the need for atmospheric propagation correction.

Key members of the TIGERISS team developing the operational plan for the mission are active researchers in the CALET collaboration and are leveraging that experience to best plan for exceptional circumstances. An FOV camera with a fisheye lens is planned for the TIGERISS payload to allow for additional monitoring of obstructions which can be removed in analysis. Due to the energy thresholds, the background radiation environment is not of concern to TIGERISS operations. Furthermore, the treatment of orientation changes will be treated on a case-by-case basis. Using this information in geomagnetic modeling of particle transport to the ISS will allow for seamless operations during these times with minimal impact to science results.

Acknowledgements

We gratefully acknowledge JAXA's contributions to the development of CALET and to the operations onboard the International Space Station. The CALET effort in Italy is supported by ASI under Agreement No. 2013- 018-R.0 and its amendments. The CALET effort in the United States is supported through Grants No. 80NSSC20K0397, No. 80NSSC20K0399, and Np. NNH18ZDA001N-APRA18-004, and under award Np. 80GSFC21M0002. This work was supported in part by JSPS Grant-in-Aid for Scientific Research (S) Grant No. 19H05608 in Japan.

References

[1] S. Torii for the CALET Collaboration, "Highlights from the CALET observations for 7.5 years on the International Space Station," this conference.

[2] Y. Asaoka et al. (CALET Collaboration), "On-Orbit Operations and Offline Data Processing of CALET Onboard the ISS," AP 100, 29–37 (2018).

[3] K. Yamaoka et al. (CALET Collaboration), "The CALET Gamma-ray Burst Monitor (CGBM)," 7th Huntsville Gamma-Ray Burst Symposium, GRB 2013, arXiv:1311.4084 (2013).

[4] N. Cannady et al. (CALET Collaboration), "Characteristics and Performance of the CALorimetric Electron Telescope (CALET) Calorimeter for Gamma-Ray Observations," ApJS 238, 5 (2018).

[5] B. Rauch et al. (TIGERISS Collaboration), "The Trans-Iron Galactic Element Recorder for the International Space Station (TIGERISS)," this conference.

Full Author List: CALET Collaboration

O. Adriani[1,2], Y. Akaike[3,4], K. Asano[5], Y. Asaoka[5], E. Berti[2,6], G. Bigongiari[7,8], W.R. Binns[9], M. Bongi[1,2], P. Brogi[7,8], A. Bruno[10], N. Cannady[11,12,13], G. Castellini[6], C. Checchia[7,8], M.L. Cherry[14], G. Collazuol[15,16], G.A. de Nolfo[10], K. Ebisawa[17], A.W. Ficklin[14], H. Fuke[17], S. Gonzi[1,2,6], T.G. Guzik[14], T. Hams[11], K. Hibino[18], M. Ichimura[19], K. Ioka[20], W. Ishizaki[5], M.H. Israel[9], K. Kasahara[21], J. Kataoka[22], R. Kataoka[23], Y. Katayose[24], C. Kato[25], N. Kawanaka[20], Y. Kawakubo[14], K. Kobayashi[3,4], K. Kohri[26], H.S. Krawczynski[9], J.F. Krizmanic[12], P. Maestro[7,8], P.S. Marrocchesi[7,8], A.M. Messineo[8,27], J.W. Mitchell[12], S. Miyake[28], A.A. Moiseev[29,12,13], M. Mori[30], N. Mori[2], H.M. Motz[18], K. Munakata[25], S. Nakahira[17], J. Nishimura[17], S. Okuno[18], J.F. Ormes[31], S. Ozawa[32], L. Pacini[2,6], P. Papini[2], B.F. Rauch[9], S.B. Ricciarini[2,6], K. Sakai[11,12,13], T. Sakamoto[33], M. Sasaki[29,12,13], Y. Shimizu[18], A. Shiomi[34], P. Spillantini[1], F. Stolzi[7,8], S. Sugita[33], A. Sulaj[7,8], M. Takita[5], T. Tamura[18], T. Terasawa[5], S. Torii[3], Y. Tsunesada[35,36], Y. Uchihori[37], E. Vannuccini[2], J.P. Wefel[14], K. Yamaoka[38], S. Yanagita[39], A. Yoshida[33], K. Yoshida[21], and W.V. Zober[9]

[1]Department of Physics, University of Florence, Via Sansone, 1 - 50019, Sesto Fiorentino, Italy, [2]INFN Sezione di Firenze, Via Sansone, 1 - 50019, Sesto Fiorentino, Italy, [3]Waseda Research Institute for Science and Engineering, Waseda University, 17 Kikuicho, Shinjuku, Tokyo 162-0044, Japan, [4]JEM Utilization Center, Human Spaceflight Technology Directorate, Japan Aerospace Exploration Agency, 2-1-1 Sengen, Tsukuba, Ibaraki 305-8505, Japan, [5]Institute for Cosmic Ray Research, The University of Tokyo, 5-1-5 Kashiwa-no-Ha, Kashiwa, Chiba 277-8582, Japan, [6]Institute of Applied Physics (IFAC), National Research Council (CNR), Via Madonna del Piano, 10, 50019, Sesto Fiorentino, Italy, [7]Department of Physical Sciences, Earth and Environment, University of Siena, via Roma 56, 53100 Siena, Italy, [8]INFN Sezione di Pisa, Polo Fibonacci, Largo B. Pontecorvo, 3 - 56127 Pisa, Italy, [9]Department of Physics and McDonnell Center for the Space Sciences, Washington University, One Brookings Drive, St. Louis, Missouri 63130-4899, USA, [10]Heliospheric Physics Laboratory, NASA/GSFC, Greenbelt, Maryland 20771, USA, [11]Center for Space Sciences and Technology, University of Maryland, Baltimore County, 1000 Hilltop Circle, Baltimore, Maryland 21250, USA, [12]Astroparticle Physics Laboratory, NASA/GSFC, Greenbelt, Maryland 20771, USA, [13]Center for Research and Exploration in Space Sciences and Technology, NASA/GSFC, Greenbelt, Maryland 20771, USA, [14]Department of Physics and Astronomy, Louisiana State University, 202 Nicholson Hall, Baton Rouge, Louisiana 70803, USA, [15]Department of Physics and Astronomy, University of Padova, Via Marzolo, 8, 35131 Padova, Italy, [16]INFN Sezione di Padova, Via Marzolo, 8, 35131 Padova, Italy, [17]Institute of Space and Astronautical Science, Japan Aerospace Exploration Agency, 3-1-1 Yoshinodai, Chuo, Sagamihara, Kanagawa 252-5210, Japan, [18]Kanagawa University, 3-27-1 Rokkakubashi, Kanagawa, Yokohama, Kanagawa 221-8686, Japan, [19]Faculty of Science and Technology, Graduate School of Science and Technology, Hirosaki University, 3, Bunkyo, Hirosaki, Aomori 036-8561, Japan, [20]Yukawa Institute for Theoretical Physics, Kyoto University, Kitashirakawa Oiwake-cho, Sakyo-ku, Kyoto, 606-8502, Japan, [21]Department of Electronic Information Systems, Shibaura Institute of Technology, 307 Fukasaku, Minuma, Saitama 337-8570, Japan, [22]School of Advanced Science and Engineering, Waseda University, 3-4-1 Okubo, Shinjuku, Tokyo 169-8555, Japan, [23]National Institute of Polar Research, 10-3, Midori-cho, Tachikawa, Tokyo 190-8518, Japan, [24]Faculty of Engineering, Division of Intelligent Systems Engineering, Yokohama National University, 79-5 Tokiwadai, Hodogaya, Yokohama 240-8501, Japan, [25]Faculty of Science, Shinshu University, 3-1-1 Asahi, Matsumoto, Nagano 390-8621, Japan, [26]Institute of Particle and Nuclear Studies, High Energy Accelerator Research Organization, 1-1 Oho, Tsukuba, Ibaraki, 305-0801, Japan, [27]University of Pisa, Polo Fibonacci, Largo B. Pontecorvo, 3 - 56127 Pisa, Italy, [28]Department of Electrical and Electronic Systems Engineering, National Institute of Technology (KOSEN), Ibaraki College, 866 Nakane, Hitachinaka, Ibaraki 312-8508, Japan, [29]Department of Astronomy, University of Maryland, College Park, Maryland 20742, USA, [30]Department of Physical Sciences, College of Science and Engineering, Ritsumeikan University, Shiga 525-8577, Japan, [31]Department of Physics and Astronomy, University of Denver, Physics Building, Room 211, 2112 East Wesley Avenue, Denver, Colorado 80208-6900, USA, [32]Quantum ICT Advanced Development Center, National Institute of Information and Communications Technology, 4-2-1 Nukui-Kitamachi, Koganei, Tokyo 184-8795, Japan, [33]College of Science and Engineering, Department of Physics and Mathematics, Aoyama Gakuin University, 5-10-1 Fuchinobe, Chuo, Sagamihara, Kanagawa 252-5258, Japan, [34]College of Industrial Technology, Nihon University, 1-2-1 Izumi, Narashino, Chiba 275-8575, Japan, [35]Graduate School of Science, Osaka Metropolitan University, Sugimoto, Sumiyoshi, Osaka 558-8585, Japan, [36]Nambu Yoichiro Institute for Theoretical and Experimental Physics, Osaka Metropolitan University, Sugimoto, Sumiyoshi, Osaka 558-8585, Japan, [37]National Institutes for Quantum and Radiation Science and Technology, 4-9-1 Anagawa, Inage, Chiba 263-8555, Japan, [38]Nagoya University, Furo, Chikusa, Nagoya 464-8601, Japan, [39]College of Science, Ibaraki University, 2-1-1 Bunkyo, Mito, Ibaraki 310-8512, Japan